

## THE FAINT SUB-MILLIMETER GALAXY POPULATION: *HUBBLE SPACE TELESCOPE* MORPHOLOGIES AND COLORS<sup>1</sup>

IAN SMAIL<sup>2,3</sup>, R. J. IVISON<sup>3,4</sup>, A. W. BLAIN<sup>5</sup> & J.-P. KNEIB<sup>6</sup>

<sup>2</sup>) Department of Physics, University of Durham, South Road, Durham DH1 3LE, UK

<sup>4</sup>) Institute for Astronomy, Dept. of Physics & Astronomy, University of Edinburgh, Blackford Hill, Edinburgh EH9 3HJ, UK

<sup>5</sup>) Cavendish Laboratory, Madingley Road, Cambridge CB3 0HE, UK

<sup>6</sup>) Observatoire Midi-Pyrénées, 14 Avenue E. Belin, F-31400 Toulouse, France

Received 1998 May 26th; accepted: 1998 --

### ABSTRACT

We present optical morphologies obtained from deep *Hubble Space Telescope* (*HST*) and ground-based images for galaxies selected from the first sub-millimeter (sub-mm) survey of the distant Universe. Our sample comprises galaxies detected in deep 850- $\mu\text{m}$  continuum maps of seven massive clusters, obtained using SCUBA, the new bolometer camera on the JCMT. The survey covers a total area of 0.01 degree<sup>2</sup> to  $1\sigma$  noise levels of about 2 mJy beam<sup>-1</sup>. We detect a total of 25 sources at 850  $\mu\text{m}$ , of which 17 and 10 are brighter than the respective 50% and 80% completeness limits. Optical counterparts are identified for 14 of the 16 sources in the  $f_{50\%}$  sample and for 9 of the 10 sources in the  $f_{80\%}$  sample that lie within our optical fields. The morphologies of those galaxies for which we have *HST* imaging fall into three broad categories: faint disturbed galaxies and interactions; faint galaxies too compact to classify reliably; and dusty, star-forming galaxies at intermediate redshifts. The disturbed and interacting galaxies constitute the largest class, which suggests that interactions remain an important mechanism for triggering star formation and the formation of ultraluminous galaxies in the distant Universe. The faint, compact galaxies may represent a later evolutionary stage in these mergers, or more centrally-concentrated starbursts. It is likely that some of these will host active galactic nuclei. Analysis of the colors of our sample allow us to estimate a crude redshift distribution:  $\gtrsim 75\%$  have  $z \lesssim 5.5$  whilst  $\gtrsim 50\%$  lie at  $z \lesssim 4.5$ , suggesting that the luminous sub-mm population is coeval with the more modestly star-forming galaxies selected by UV/optical surveys of the distant Universe. This imposes important constraints on models of galaxy formation and evolution.

*Subject headings:* cosmology: observations — cosmology: early universe — galaxies: evolution — galaxies: formation — galaxies: morphology

### 1. INTRODUCTION

Recent technological advances in ground-based sub-mm technology (Holland et al. 1998) are set to revolutionise our understanding of the star-formation history of galaxies (Blain et al. 1998a, BSIK). Deep maps of the sub-mm sky (Smail, Ivison & Blain 1997, SIB) have now resolved the population of galaxies responsible for the far-infrared background (Puget et al. 1996; Fixsen et al. 1998; Schlegel, Finkbeiner & Davis 1998) and offer a precise determination of the star-formation rate (SFR) in distant, dust-obscured systems (e.g. Dey et al. 1998). This population is responsible for a substantial fraction of the total SFR in the early Universe (BSIK) and holds crucial information about how galaxies formed and evolved (Blain & Longair 1993).

Our sub-mm survey, the first results of which were reported by SIB, exploits massive, foreground clusters to enhance the sensitivity of the maps to distant star-forming galaxies (Blain 1997). The survey has now been extended to cover seven clusters (Smail et al. 1998b, S98) with sufficient sensitivity to detect a luminous infrared galaxy such as Arp 220 out to  $z \sim 10$ . Our sub-mm galaxy counts greatly exceed those expected in a non-evolving model based on the local *IRAS* 60- $\mu\text{m}$  luminosity function (Saunders et al. 1990), or in a model that can explain the

optically-selected Lyman-dropout (Madau et al. 1996) and Lyman-emission samples (Hu, Cowie & McMahan 1998).

As demonstrated by BSIK, before we can understand the star-formation history of the Universe, we need one remaining piece of the puzzle: the redshift distribution,  $N(z)$ , of a faint sub-mm-selected galaxy sample. The identification of the complete S98 catalog is underway (Ivison et al. 1998a), this benefits from archival *HST* images for most of the survey area as well as the availability of 10- $\mu\text{Jy}$  beam<sup>-1</sup> radio maps for all the fields (Ivison et al. 1998b). In the meantime, useful limits on the sub-mm  $N(z)$  can be determined from broad-band imaging (Steidel et al. 1996). Even a basic analysis along these lines can challenge some currently viable models of galaxy evolution (BSIK).

In this paper we present limits on the redshift distribution of a sample of sub-mm-selected galaxies derived from deep optical imaging. We also take advantage of archival *HST* images to investigate the optical morphologies for a sub-sample of our catalog on angular scales down to 0.1 arcsec ( $\lesssim 1h_{50}^{-1}$  kpc at the expected redshifts). This detailed morphological information can provide a valuable insight into the physical mechanisms responsible for the high SFR of these distant galaxies and thereby providing a fuller understanding of the early stages of galaxy forma-

<sup>1</sup>Based on observations with the NASA/ESA *Hubble Space Telescope* obtained at the Space Telescope Science Institute, which is operated by the Association of Universities for Research in Astronomy Inc., under NASA contract NAS 5-26555.

<sup>3</sup>PPARC Advanced Fellow.

Table 1  
Log of the SCUBA observations

Cluster	R.A. (J2000)	Dec. (J2000)	$z$	Exposure time (ks)	$f_{850}(50\%)$ (mJy)	$f_{850}(80\%)$ (mJy)	N ( $f_{850} > f_{lim}$ ) 50%	80%
Cl0024+16	00 26 35.80	+17 09 41.0	0.39	15.6	4.6	6.4	4	1
A370	02 39 53.00	-01 35 06.0	0.37	33.8	5.7	7.2	3	3
MS0440+02	04 43 09.00	+02 10 19.9	0.19	35.8	4.4	6.0	2	1
Cl0939+47	09 42 56.38	+46 59 10.4	0.40	30.1	5.8	7.4	1	1
A1835	14 01 02.20	+02 52 43.0	0.25	23.0	5.0	6.6	3	2
A2390	21 53 36.89	+17 41 45.8	0.23	33.7	6.6	7.9	2	1
Cl2244-02	22 47 11.90	-02 05 38.0	0.33	25.6	5.1	6.7	2	1

tion and evolution.

## 2. OBSERVATIONS, REDUCTION AND ANALYSIS

### 2.1. Sub-millimeter Observations

Our 850- $\mu\text{m}$  maps were constructed using the long-wavelength array of the Sub-millimeter Common-User Bolometer Array (SCUBA, Robson et al. 1998) on the James Clerk Maxwell Telescope (JCMT)<sup>8</sup>. The final on-source integration times and field centers are listed in Table 1. Each field covers an area of 5.2 arcmin<sup>2</sup>, giving a total survey area of 0.01 degree<sup>2</sup>. The typical amplification for background sources detected in our fields is expected to be  $1.5^{+5.0}_{-0.5}$ , and so we have in effect surveyed an area of about 25 arcmin<sup>2</sup> in the source plane to an equivalent  $1\sigma$  sensitivity of 1.3 mJy.

Source catalogs were constructed using the SExtractor package (Bertin & Arnouts 1996) and Monte Carlo incompleteness simulations undertaken as described in SIB, for more details see Blain et al. (1998b) and S98. The derived sensitivity limits, 850- $\mu\text{m}$  fluxes ( $f_{850}$ ) for 50% and 80% completeness of  $f_{850}(50\%)$  and  $f_{850}(80\%)$ , and the number of detected sources in each field are listed in Table 1. We identify only two sources by applying the same selection criteria to the negative fluctuations in our maps, both have  $f_{850} < f_{850}(50\%)$ , indicating a false detection rate in our full catalog of  $\lesssim 10\%$ . In the remainder of our analysis we will focus on the two sub-samples from our full catalog of 25 sources: 10 sources with  $f_{850} > f_{850}(80\%)$  which we will denote  $f_{80\%}$  and a slightly more liberal sub-sample ( $f_{50\%}$ ) defined by  $f_{850} > f_{850}(50\%)$  and containing 17 sources. The  $f_{80\%}$  and  $f_{50\%}$  limits are roughly equivalent to 4- and 3- $\sigma$  of the sky noise.

### 2.2. Archival Optical Observations

In Table 2 we list the *HST* WFPC2 and the wider-field, ground-based observations used in our analysis. The WFPC2 observations are mainly from programs with which we are associated; the remainder were retrieved from the ST-ECF archive. All were reduced as described by Smail et al. (1997). For one cluster, Cl0939+47, we have used the deconvolved pre-refurbishment WF/PC-1 images of Dressler et al. (1994) to determine the morphologies for SCUBA sources lying outside the WFPC2 field of view. The ground-based observations come from a variety of sources, predominantly from programs on the 3.6-m CFHT (Kneib et al. 1993) and the 5.1-m Hale (Dressler & Gunn 1992; Smail et al. 1998a). The reduction and calibration

of these images is documented in those papers. While lacking the spatial resolution and depth of the WFPC2 images, these data have a wider field of view and a more comprehensive wavelength coverage.

Total magnitudes for all the sub-mm-selected galaxies covered by our optical images were estimated using SExtractor’s BEST\_MAG in the reddest passband available for each cluster (either  $R$  or  $I$ ), using *HST* frames if available. Galaxy colors were measured within 1-arcsec diameter apertures on the WFPC2 frames and 3-arcsec apertures on the ground-based images, after matching the effective seeing on the different frames. If required, the photometry was converted to the  $I$ -band assuming  $(R - I) \sim 0.5 \pm 0.2$ , which is typical of both the faint field population (Smail et al. 1995) and the available photometry for our sub-mm counterparts. For Cl0939+47, the  $(g - i)$  colors from Dressler & Gunn (1992) were transformed to  $(V - I)$  (Kent 1985). No reddening corrections were applied.

### 2.3. Optical Identifications

The absolute positional accuracy of the SCUBA maps is better than 3 arcsec, as estimated from repeated pointing checks performed during the observations. The positions of detected sources were determined by fitting a circular gaussian to a 30-arcsec diameter region (two beam widths) around the peak flux position on 4-arcsec-sampled maps. The random errors in the positions of individual objects depend on the signal-to-noise ratio of the detections, but should be no worse than 4 arcsec rms for the faintest sources discussed here. The combined positional uncertainty of our faintest sub-mm sources is therefore  $\lesssim 6$  arcsec (c.f. Fig. 1, Plate. 1). Counterparts were sought within this radius of the nominal sub-mm position.

Using the deepest and/or reddest passband available for each cluster, we identified all counterparts down to the magnitude limits of our optical data for the 25 sub-mm sources from the full catalog. These limits are typically  $I \sim 23.5$  and 26.0 for the ground-based and *HST* exposures respectively. Ten sources in the  $f_{80\%}$  sample lie within our optical images; 7 of these are on the *HST* frames and the remaining 3 on ground-based images. The equivalent numbers for the 16 source in the  $f_{50\%}$  sample are 11 and 5. In two maps a *bright* sub-mm source has a clear counterpart, and so their coordinates were corrected to align the sources exactly.

Due to the nature of sub-mm-selected galaxies, the optical counterparts are likely to be faint, moreover the cluster fields analysed here are crowded. Thus in some instances there is a non-zero likelihood of an unrelated galaxy falling

<sup>8</sup>The JCMT is operated by the Observatories on behalf of the UK Particle Physics and Astronomy Research Council, the Netherlands Organization for Scientific Research and the Canadian National Research Council.

Table 2  
Log of archival optical observations

Cluster	<i>HST</i> /WFPC2 (Filter [Exposure time/ks])	Reference	Ground-based	Reference
Cl0024+16	F450W [23.4] F814W [13.2]	Smail et al. (1997)	<i>I</i>	Mellier (priv. comm.)
A370	F336W [27.8] F675W [5.6]	Archive	<i>UBVRI</i>	Kneib et al. (1993)
MS 0440+02	F702W [18.4]	Archive	...	...
Cl 0939+47	F702W [21.0] F702W [22.0] <sup>a</sup>	Smail et al. (1997)	<i>gri</i>	Dressler & Gunn (1992)
A1835	...	...	<i>UBI</i>	Smail et al. (1998)
A2390	F555W [8.4] F814W [10.5]	Kneib et al. (1998)	<i>UBI</i>	Smail et al. (1998)
Cl2244-02	F555W [8.4] F814W [10.5]	Archive	...	...

a) WF/PC-1 observations, reduced and deconvolved as described in Dressler et al. (1994)

within the sub-mm error box. As such our identifications should be treated as preliminary until they have been confirmed from deep radio maps, in particular it is possible that in a small number of cases we have misidentified a sub-mm source due to the faintness of the true counterpart combined with the presence of a nearby, brighter galaxy. Nevertheless, as we show below the majority of the identified counterparts are likely to be real and so the broad characteristics of luminous sub-mm galaxies can be ascertained from our current catalog.

The likelihood of a false identification for a given sub-mm source will be a function of both the apparent magnitude of the identified counterpart and its distance from the nominal position of the sub-mm source. We have used this information to estimate the probability of a real association on an object-by-object basis. Using a Monte Carlo simulation, based upon the observed number counts of galaxies within each of our optical images, we estimate the probability of a galaxy with the observed apparent magnitude (or brighter) falling at random within a circle defined by the optical and sub-mm positions. The reliability of an identification have been assigned to one of four classes based upon the probability of a chance coincidence  $P$ :  $P \leq 0.01$ , definite;  $P \leq 0.10$ , likely;  $P \leq 0.25$ , possible and  $P \geq 0.25$ , blank field.

### 3. RESULTS AND DISCUSSION

The aim of this work is to obtain a first view of the optical properties of the galaxies which contribute a substantial fraction of the sub-mm emission in the Universe. To this end we retain the  $f_{50\%}$  sample although it is not statistically complete, instead we use it to provide support for any trends seen in the smaller  $f_{80\%}$  sample. In the  $f_{80\%}$  sample of 10 sources within the optical fields, there are 4 counterparts with  $P \leq 0.0$ , 9 with  $P \leq 0.25$  and 1 blank field. The rms offset between sub-mm sources and the 9 counterparts is  $2.3 \pm 0.5$  arcsec, in reasonable agreement with the nominal positional accuracy of the SCUBA maps. The 16 sources with  $f_{850} > f_{850}(50\%)$  are associated with 6 definite identifications, 8 likely/possible identifications and 2 blank fields.

In the following discussion we use all counterparts with  $P \leq 0.25$ , noting that none of our conclusions are substantially altered if we restrict our sample to those counterparts with  $P \leq 0.10$ .

Multicolor photometry is available for 9 of the 10 sources in the  $f_{80\%}$  sample (12/16 in the  $f_{80\%}$ ). One of these 9 fields is blank and in the remaining 8 we have 6  $B$  and 2  $V$ -band detections. For the more liberal  $f_{50\%}$  sample we have 8  $B$ -band and 4  $V$ -band detections from a total of

12 identified sources with multicolor photometry. In all instances where we have both  $B$  and  $V$ -band data, the counterpart galaxies are detected in both bands. The galaxies plotted in Fig. 2 have a broad apparent-magnitude distribution and span the whole range of colors seen in the faint field population. We find no strong correlation between sub-mm flux and  $I$ -band magnitude, as expected due to the wider selection function of a sub-mm survey compared with that of optical surveys.

The detection of a galaxy in one of the bluer passbands can be used to impose an upper limit to its redshift, because of the strong absorption by the foreground Lyman- $\alpha$  forest at rest-frame wavelengths shortward of 912Å. Thus the number of detections in the  $B$ - and  $V$ -band images requires that at least 8/10 or  $\gtrsim 80\%$  of the galaxies in our  $f_{80\%}$  sample have  $z \lesssim 5.5$ , the redshift at which the Lyman-limit moves through the  $V$ -band. At least half of this sample lies at  $z \lesssim 4.5$  based on the  $B$ -band data alone. The equivalent limits for the  $f_{50\%}$  sample are  $\gtrsim 75\%$  at  $z \lesssim 5.5$  and  $\gtrsim 50\%$  with  $z \lesssim 4.5$ . Thus these luminous sub-mm galaxies appear to span a similar redshift range to that covered by the more modestly star-forming galaxies selected in UV/optical surveys of the distant Universe (Madau et al. 1996).

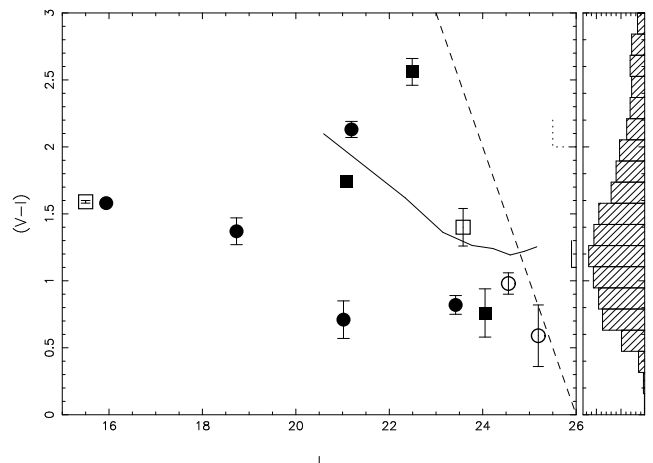


Fig. 2. The  $(V-I)-I$  color-magnitude diagram for the 18 SCUBA sources for which we have multi-color information, the approximate limits for the 2 non-detections are marked. The filled symbols and solid limits show those sources in the  $f_{80\%}$  sample, the open points and dotted limits are the remaining  $f_{50\%}$  sources. The square symbols represent  $(B-I)$  measurements converted to  $(V-I)$  assuming  $(B-V) = 0.5$ . The apparent magnitudes of the background sources have been corrected for a mean amplification of 1.5. The dashed line shows the effective completeness limit in our optical images. The solid line indicates the median  $(V-I)$  color as a function of  $I$  magnitude for the faint field population, and the histogram gives the distribution of  $(V-I)$  colors for a sample of field galaxies down to  $I = 25$  (Smail et al. 1995).

The range of evolutionary models that can account for

all the sub-mm and far-infrared data currently available (BSIK) can already be constrained by these crude limits. We can reject any model which predicts that more than  $\sim 20\%$  of galaxies selected at an  $850\text{-}\mu\text{m}$  flux limit of  $3\text{ mJy}$  lie beyond  $z \sim 5.5$ .

Turning to the morphological composition of our catalog, we have used high-quality *HST* images to provide detailed morphologies for the 11 sub-mm-selected galaxies within these fields (Fig. 1). For the remaining 5 objects we use ground-based images, with typically sub-arcsec resolution, to make cruder classifications. Across the whole catalog we find that the morphologies of the sub-mm galaxies can be split roughly into 3 classes: 1) faint, disturbed galaxies, some of which are obviously undergoing mergers and interactions; 2) faint, compact galaxies, too small to classify reliably; and 3) bright, dusty star-forming galaxies. We define a disturbed galaxy on the basis of the presence of one or more of the following; multiple components, close companions with similar sizes and colors, clearly distorted morphologies or tidal extensions. Some of these signatures are only visible on scales of  $\lesssim 1$  arcsec in the *HST* images, and so there is an obvious bias against identifying such systems in our ground-based data. The morphologies of the 9 identified counterparts in the  $f_{80\%}$  sample fall into the three classes in the ratio 5(2):1(1):3(0), numbers in parentheses give the values from the ground-based observations. The corresponding ratios for the 14 optical counterparts in the  $f_{850} > f_{850}(50\%)$  sample are 6(3):4(1):4(1).

The bright galaxies, shown in the bottom row of Fig. 1, include two central galaxies from the clusters used in our survey. These clusters both contain strong cooling flows and their central galaxies show signatures of strong star-formation activity and some non-thermal emission. The properties of these two galaxies are investigated in more depth in a forthcoming paper. As confirmed cluster members these two galaxies are removed from the analysis here. The remaining 2 bright galaxies are both dusty Sab–Sbc spirals, lying at intermediate redshifts, within or in front of the clusters. The flux density limit of our  $850\text{-}\mu\text{m}$  survey means that we would expect to detect this type of galaxy, with a  $\text{SFR} \gtrsim 20\text{--}50 M_{\odot}\text{yr}^{-1}$ , at  $z \lesssim 0.2\text{--}0.5$ . We note that none of these bright galaxies was included in the analysis of SIB.

The optically faint sources are most interesting, as they typically lie at high redshifts and have high SFRs,  $\gtrsim 100 M_{\odot}\text{yr}^{-1}$ . The number of these galaxies that are clearly disturbed/interacting systems is roughly equal to the number that are either too faint or too compact to be classified reliably. This is a very robust result – at least 50% of our faint, distant sub-mm-selected sources are identified with distorted or interacting galaxies. This interaction rate is higher than the 30% seen in the general field population at a similar magnitude limit (van den Bergh et al. 1996). The median separation of the observed components in the interacting systems is about  $10h_{50}^{-1}\text{ kpc}$ . 50%

is thus a firm lower limit to the fraction of interactions as some of the more compact sources, with typical half-light radii of  $0.2\text{--}0.4$  arcsec, or  $2\text{--}4h_{50}^{-1}\text{ kpc}$  at  $z > 1$ , may be either unresolved or more evolved mergers. The exact nature of the compact galaxies will require further investigation, in particular we are obtaining high-resolution near-infrared images to provide a more representative view of these galaxies.

Strong interactions and mergers are mechanisms responsible for the high SFRs of ultraluminous infrared galaxies (ULIRG) in the local Universe (Sanders & Mirabel 1996). The fraction of interacting ULIRGs found locally is comparable to or greater than our lower limit, but the mean separation of the components is close to the resolution limit of even our WFPC2 images. Hence we suggest that the rate of interaction found in our distant, sub-mm-selected galaxies is probably comparable to that seen in local ULIRGs. On the basis of our morphological survey we can state that one mechanism, dynamical interaction, is responsible for triggering at least half of the sub-mm flux density, and by implication for at least half of the star-formation activity in the most distant strongly star-forming galaxies in our sample. These observations provide the clearest support for the pivotal role of mergers and interactions in the early evolution of luminous star-forming galaxies.

#### 4. CONCLUSIONS

- We present optical identifications of galaxies selected in a deep sub-mm survey. Roughly 70% of the sources selected at  $850\text{ }\mu\text{m}$ , for which optical imaging data is available, have definite/likely counterparts. A further 20% of the sub-mm sources have probable optical counterparts, only 20% of the sub-mm sources have no identifiable counterpart to a typical apparent magnitude of  $I \sim 25\text{--}26$ .
- 75% of the optical counterparts for which we have *B* or *V*-band images are detected in these passbands, suggesting that at least three-quarters of the  $850\text{-}\mu\text{m}$ -selected galaxies brighter than  $3\text{ mJy}$  lie at  $z \lesssim 5.5$ .
- The morphologies of the fainter (and hence probably more distant) optical counterparts fall roughly equally into two classes: disturbed/interacting and compact objects. The prevalence of interactions in this survey underlines the central role of this mechanism in triggering star-formation in the most luminous galaxies at high redshift.

#### ACKNOWLEDGEMENTS

We thank the commissioning team of SCUBA and Ian Robson for his continuing support. We also thank Yannick Mellier for allowing us to use his exquisite CFHT images of C10024+16, and Wayne Holland, Tim Jenness, Malcolm Longair and Michael Rowan-Robinson for useful conversations and help. IRS acknowledges support from the Royal Society and the Australian Research Council while a Visiting Fellow at UNSW, Sydney.

#### REFERENCES

- Bertin, E., Arnouts, S., 1996, *A&A*, 117, 393  
 Blain, A. W., 1997, *MNRAS*, 283, 1340  
 Blain, A. W., Smail, I., Ivison, R. J., Kneib, J.-P., 1998a, *MNRAS*, submitted. (BSIK)  
 Blain, A. W., Kneib, J.-P., Ivison, R. J., Smail, I., 1998b, in prep.  
 Blain, A. W., Longair, M. S., 1993, *MNRAS*, 264, 509.  
 Cimatti, A., Andreani, P., Rottgering, H., Tilanus, R., 1998, *Nature*, in press (astro-ph/9804302)  
 Dey, A., Graham, J., Ivison, R. J., Smail, I., 1998, in prep.  
 Dressler, A., Gunn, J. E., 1992, *ApJS*, 78, 1.  
 Dressler, A., Oemler, A., Butcher, H., Gunn, J. E., 1994, *ApJ*, 430, 139.

Fixsen D. J., Dwek E., Mather J. C., Bennett C. L., Shafer R. A., 1998, *ApJ*, submitted (astro-ph/9803021)  
 Holland, W. S., Gear, W. K., Lightfoot, J. F., Jenness, T., Robson, E. I., Cunningham, C. R., et al., 1998, preprint.  
 Hu, E. M., Cowie, L. L., McMahon, R. G., 1998, preprint (astro-ph/9803011)  
 Ivison, R. J., Smail, I., Le Borgne, J.-F., Blain, A. W., Kneib, J.-P., et al., 1998a, *MNRAS*, in press (astro-ph/9712161).  
 Ivison, R. J., Owen, F., Smail, I., Blain, A. W., Kneib, J.-P., 1998b, *ApJ*, in prep.  
 Kent, S. M., 1995, *PASP*, 97, 165.  
 Kneib, J.-P., Mellier, Y., Fort, B., Mathez, G., 1993, *A&A*, 273, 367.  
 Kneib, J.-P., Pelló, R., Mellier, Y., Soucail, G., Fort, B., et al., 1998, in prep.  
 Madau, P., Ferguson, H. C., Dickinson, M. E., Giavalisco, M., Steidel, C. S., Fruchter, A., 1996, *MNRAS*, 283, 1388.  
 Puget J.-L., Abergel A., Bernard J.-P., Boulanger F., Burton W. B., et al., 1996, *A&A*, 308, L5

Robson, E. I. et al., 1998, *MNRAS*, in prep.  
 Sanders, D. B., Mirabel, I. F., 1996, *ARAA*, 34, 749.  
 Saunders W., Rowan-Robinson M., Lawrence A., Efstathiou G., Kaiser N., et al., 1990, *MNRAS*, 242, 318.  
 Schlegel, D. J., Finkbeiner, D. P., Davis, M., 1998, *ApJ*, 499, in press. (astro-ph/9710327)  
 Smail, I., Hogg, D. W., Yan, L., Cohen, J. G., 1995, *ApJL*, 449, L105.  
 Smail, I., Dressler, A., Couch, W. J., Ellis, R. S., Oemler, A., et al., 1997, *ApJS*, 110, 213.  
 Smail, I., Ivison, R. J., Blain, A. W., 1997, *ApJL*, 490, L5. (SIB)  
 Smail, I., Edge, A. C., Ellis, R. S., Blandford, R. D., 1998a, *MNRAS*, 293, 124.  
 Smail, I., et al., 1998b, in prep. (S98)  
 Steidel C. C., Giavalisco M., Dickinson M., Adelberger K. L., 1996a, *AJ*, 112, 352.  
 van den Bergh, S., Abraham, R. G., Ellis, R. S., Tanvir, N. R., Santiago, B. X., Glazebrook, K. G., 1996, *AJ*, 112, 359.

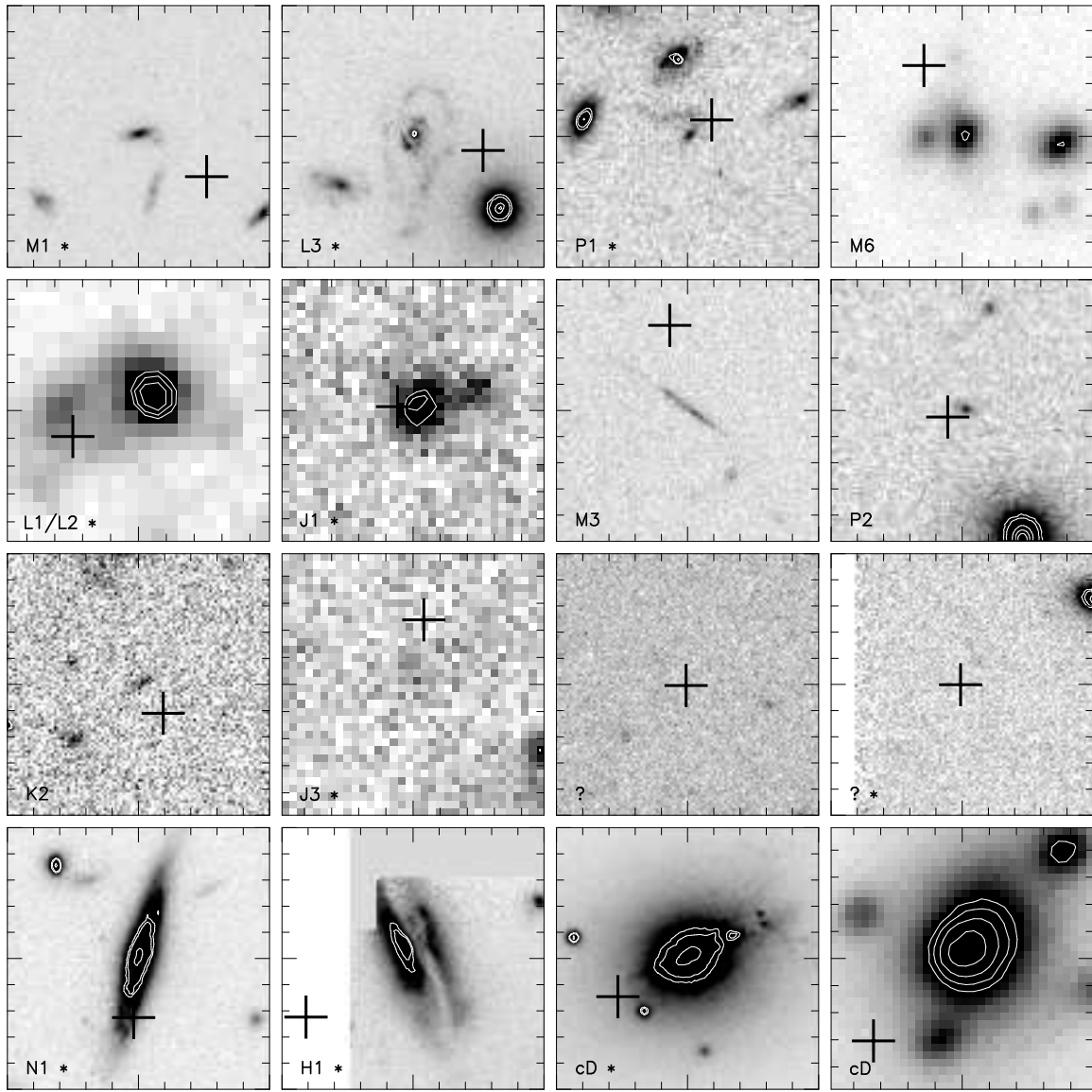


Fig. 1.  $10 \times 10$  arcsec images of the 16 sub-mm sources in our  $f_{50\%}$  sample which fall within our optical imaging of the seven clusters. These are ordered from the upper-left on the basis of their morphologies: 6 disturbed/interacting, 4 compact/featureless (including a strongly-distorted arclet), 2 blank fields and then 4 bright, dusty galaxies. A '?' next to the sub-mm source name indicates a blank field, a '\*' marks those sub-mm sources for which  $f_{850} > f_{850}(80\%)$ . The images are centred on the most likely optical candidate. The centroids of the sub-mm sources are indicated by crosses. Note that these images span a range in exposure times and resolutions (Table 2). The panels correspond to  $\gtrsim 80h_{50}^{-1}$  kpc at  $z > 1$ .